PLOS ONE

Regulation of Action Potential Waveforms by Axonal GABA_A Receptors in Cortical Pyramidal Neurons

Yang Xia[1], Yuan Zhao[2], Mingpo Yang[1], Shaoqun Zeng[2]*, Yousheng Shu[3]*

1 Institute of Neuroscience, State Key Laboratory of Neuroscience, Shanghai Institutes for Biological Sciences, Chinese Academy of Sciences, Shanghai, P. R. China, 2 Britton Chance Center for Biomedical Photonics, Wuhan National Laboratory for Optoelectronics-Huazhong University of Science and Technology, Wuhan, P. R. China, 3 State Key Laboratory of Cognitive Neuroscience and Learning & IDG/McGovern Institute for Brain Research, Center for Collaboration and Innovation in Brain and Learning Sciences, Beijing Normal University, Beijing, P. R. China

Abstract

GABA_A receptors distributed in somatodendritic compartments play critical roles in regulating neuronal activities, including spike timing and firing pattern; however, the properties and functions of GABA_A receptors at the axon are still poorly understood. By recording from the cut end (bleb) of the main axon trunk of layer –5 pyramidal neurons in prefrontal cortical slices, we found that currents evoked by GABA iontophoresis could be blocked by picrotoxin, indicating the expression of GABA_A receptors in axons. Stationary noise analysis revealed that single-channel properties of axonal GABA_A receptors were similar to those of somatic receptors. Perforated patch recording with gramicidin revealed that the reversal potential of the GABA response was more negative than the resting membrane potential at the axon trunk, suggesting that GABA may hyperpolarize the axonal membrane potential. Further experiments demonstrated that the activation of axonal GABA_A receptors regulated the amplitude and duration of action potentials (APs) and decreased the AP-induced Ca^{2+} transients at the axon. Together, our results indicate that the waveform of axonal APs and the downstream Ca^{2+} signals are modulated by axonal GABA_A receptors.

Data Availability: The authors confirm that all data underlying the findings are fully available without restriction. All relevant data are within the paper and its Supporting Information files.

Competing Interests: The authors have declared that no competing interests exist.

* Email: yousheng@bnu.edu.cn (YS); sqzeng@hust.edu.cn (SZ)

Introduction

In general, the dendrites and cell body receive and summate synaptic inputs, whereas the axon is responsible for action potential (AP) initiation and propagation. The axon usually functions as a reliable cable conducting APs in all-or-none (digital) mode; however, this long-held view of the axon has recently been challenged Emerging evidences has shown that subthreshold changes in presynaptic membrane potential (V_m) can regulate the amplitude of AP-triggered postsynaptic responses, indicating that neurons also communicate in an analog mode [1,2,3]. This mode of neuronal communication may result from activities of axonal ion channels [4,5] and receptors [6,7] that regulate AP waveforms, presynaptic Ca^{2+} signals and, thus, neurotransmitter release [8,9].

Ionotropic GABA_A receptors are one of the most important components involved in the operation of neural circuits in the central nervous system (CNS) [10]. These ligand-gated receptors are heteropentamers selectively permeable to Cl^- (predominantly) and HCO_3^- [11]. Previous studies demonstrated that somatodendritic GABA_A receptors could regulate neuronal excitability, spike timing and firing pattern [12,13]. Also there were several lines of evidence implicating a role for axonal GABA_A receptors in regulating neuronal activities [14,15].

During development of the vertebrate brain, the effect of GABA_A receptor activation on V_m switches from depolarization to characteristic hyperpolarization. This transition is attributable to a decrease in the concentration of intracellular Cl^- ([Cl^-]_i), resulting from changes in the expression level of cation–chloride co-transporters such as NKCCs (Na^+-K^+-$2Cl^-$ co-transporters) and KCCs (K^+-$2Cl^-$ co-transporters) [16]. It has been reported that interneurons exert a hyperpolarizing action along the entire somatodendritic axis and the axon initial segment (AIS) of CA1 hippocampal pyramidal cells [17]. However, GABA release from axo-axonic synapses onto the AIS depolarizes cortical pyramidal cells [15]. In addition, GABA_A receptors on hippocampal mossy fibers could depolarize presynaptic boutons, enhance neurotransmission and facilitate LTP induction [18]. Another study in cerebellar granule cells also showed an increase in spike reliability and release probability after activation of axonal GABA_A receptors [19]. In these studies, noninvasive approaches such as extracellular recording, cell-attached or gramicidin perforated patch recording were employed to maintain the intracellular milieu and reveal the actual function of GABA_A receptors under physiological conditions.

In this study, we performed direct whole-cell recording from axon blebs of layer –5 pyramidal cells to investigate the role of GABA_A receptors located at the main axon trunk in regulating

neuronal signaling. Using gramicidin perforated patch recording from axonal blebs (>100 µm away from the soma), we found that the reversal potential of the GABA-mediated response was more negative than the resting V_m of the axon, suggesting that the activation of axonal GABA$_A$ receptors could cause hyperpolarization in distal axons. In addition, we show that the GABA-induced shunting and hyperpolarizing effect can shape AP waveforms and thereby AP-triggered Ca^{2+} signals at the axon.

Materials and Methods

Animals

The care and use of animals complied with the guidelines of the Animal Advisory Committee at the Shanghai Institutes for Biological Sciences. This committee also approved this research. All efforts were made to minimize animal suffering and reduce the number of animals used.

Slice Preparation

Coronal slices from prefrontal cortex were prepared from Sprague-Dawley rats (postnatal day 15–22, male). After sodium pentobarbital (30 mg/kg, i.p.) anesthesia, the animal was euthanized by decapitation. The brain was then dissected out and immersed in the following slicing solution. Slices (350–400 µm in thickness) were cut on a vibroslicer (Leica Instruments) in ice-cold slicing solution containing (in mM): 2.5 KCl, 1.25 NaH$_2$PO$_4$, 26 NaHCO$_3$, 2 MgSO$_4$, 2 CaCl$_2$, 25 dextrose, 213 sucrose (315–325 mOsm, pH 7.2–7.3). After slicing, individual slices were then transferred to an incubation chamber filled with normal ACSF similar to the slicing solution but with sucrose replaced by 126 mM NaCl. Slices were then maintained in this chamber at 34.5°C for approximately 1 hour before use. For electrophysiological experiments, slices were placed in a recording chamber and perfused with the normal ACSF (36–36.5°C). All solutions were oxygenated with carbogen gas (95% O$_2$ and 5% CO$_2$). Cortical neurons were visualized with an upright infrared differential interference contrast (IR-DIC) microscope (BX51WI; Olympus).

Electrophysiological Recordings

Whole-cell recordings were obtained from both the somata and the axonal blebs of layer –5 regular-spiking pyramidal neurons in prefrontal cortical slices [2,5]. The patch pipettes had open-tip resistances of 3–6 MΩ for somatic and 8–12 MΩ for axonal recordings. In this study, we used five types of intracellular solution (ICS) for different experiments (see below). The low-Cl$^-$ intracellular solution (low-Cl$^-$ ICS) contained (in mM): 140 K gluconate, 3 KCl, 2 MgCl$_2$, 2 Na$_2$ATP, 10 HEPES, and 0.2 EGTA (280–290 mOsm, pH 7.2 adjusted with KOH). Alexa Fluor 488 (100 µM) and Biocytin (0.2%) were also added to the ICS for visualizing the cell morphology during and after recording. The low-Cl$^-$ ICS was used in most of our experiments unless otherwise stated. The resistance of sharp electrodes for GABA iontophoresis was 30–50 MΩ when filled with 500 mM GABA (pH 3.6). During the experiments, a retention current (−10 nA) was applied to prevent passive leakage of GABA. Currents were sampled at 20 kHz and low-pass filtered at 3 kHz. AP waveforms recorded in current-clamp mode were sampled at 50 kHz and low-pass filtered at 30 kHz.

To exclude the contribution of somatodendritic GABA receptors, we performed recordings from axon blebs isolated from the soma. Isolated axon blebs could be obtained by sweeping a sharp electrode at the border between layer –6and the white matter [20]. We then recorded axonal blebs in the white-matter side. Data collected from blebs that were disconnected from the soma but attached with segments of the axon (usually tens of micrometers) were chosen for analysis. Similarly, Alexa Fluor 488 and Biocytin were added to the ICS to confirm that the blebs were indeed isolated from the soma. CsCl-based ICS containing 2 mM TEA and 145 mM CsCl (replacing K gluconate and KCl in the low-Cl$^-$ ICS) were used in this experiment.

Patch pipette solution for gramicidin perforated patch recording contained (in mM) 140 KCl, 10 NaCl, 10 HEPES (pH = 7.2 adjusted with KOH). Gramicidin was first dissolved in DMSO to prepare a stock solution and then diluted to a final concentration of 10 µg ml^{-1} (soma) or 100 µg ml^{-1} (bleb) in the pipette solution. The gramicidin-containing solution was prepared and sonicated immediately before the experiment. To facilitate the formation of a tight seal, the tip of the pipette was dipped into and filled with a gramicidin-free solution, and then the patch pipette was backfilled with a gramicidin-containing solution. After 10–20 minutes in the cell-attached configuration, the series resistance decreased and stabilized at 100–200 MΩ (soma) or 150–300 MΩ (bleb). The series resistance was monitored during all recording sessions. Alexa Fluor 488 was also added to this pipette solution for monitoring the integrity of perforated recording. The recording was terminated upon rupture of the patch membrane, as indicated by the presence of fluorescence in the recorded cell, a sudden decrease in series resistance or a dramatic change in reversal potential.

In experiments using extracellular stimulation to evoke APs, we placed a concentric electrode at layer 2/3 near the recorded cell and delivered single electrical shocks (0.1–0.3 ms in duration) to the slice. Low-Cl$^-$ ICS, modified -ICS and high-Cl$^-$ ICS were used in these experiments. In the modified -ICS, the concentration of K gluconate and KCl were adjusted to 127 and 16 mM, respectively. For high-Cl$^-$ ICS, they were adjusted to 72 and 71 mM, respectively.

We employed a MultiClamp 700B amplifier (Molecular Devices) for patch-clamp recording and Spike2 software (Cambridge Electronic Design) for data acquisition. The series resistance and capacitance were compensated before and after every experimental protocol. AxoClamp 900A (Molecular Devices) was used for GABA iontophoresis (200 nA, 2–5 ms) and Picospritzer III (Parker Hannifin Corporation) was used for local puffing of baclofen (10–30 psi, 15–20 ms). The V_m shown in the text and figures were not corrected with a liquid junction potential unless otherwise stated.

GABA, Picrotoxin (PTX), baclofen, CGP 35348, muscimol and Biocytin were obtained from Tocris; gramicidin from Sigma; Alexa Fluor 488, Alexa Fluor 594 and OGB-1 from Invitrogen.

Stationary noise analysis

The membrane currents recorded in voltage-clamp mode were sampled at 20 kHz and low-pass filtered at 6 kHz; then, the current traces were used for noise analysis. For stationary noise analysis, currents were first low-pass filtered at 400 Hz using FIR digital filtering and then transformed into AC signals using DC remove with a time constant of 1 s (Spike2 software). From each recording, we chose two segments (20–40 s) of the current trace before and during drug application.

The variance of membrane current σ_i^2 was calculated from the AC signals using the following formula:

$$\sigma_i^2 = \frac{1}{(N-1)}\sum_{k=1}^{N}(i_k - \bar{i})^2$$

where N is the total number of points in each data segments, i_k is the individual data point and $\bar{i}$ is the mean value of the current.

Subtraction of the variance under control condition from those obtained during drug application produced the drug-induced variance. The average conductance of a single channel γ can be calculated from equation $\gamma = \sigma_i^2/(\varDelta I \cdot V_D)$, where σ_i^2 is the drug-induced variance, $\varDelta I$ is the drug-induced change of the membrane current and V_D is the driving force.

Power spectra of current fluctuations were calculated as the average of fast Fourier transform of subsamples of the membrane current. Each subsample lasted for 2 s. Subtraction of baseline values from those obtained during drug application yielded the power spectra of drug-induced fluctuations. In most cases, the drug-induced spectra could be fitted by a double Lorentzian equation of the form

$$S(f) = \sum_{i=1}^{2} S_i(0)/\left(1 + \left(\frac{f}{f_i}\right)^2\right)$$

where $S_i(0)$ is the zero frequency asymptote value and f_i is the cut-off frequency of each component. The corresponding time constant τ_i is derived from $\tau_i = 1/(2\pi f_i)$. More details can be found in previous reports [21,22].

In the experiments for stationary noise analysis, in addition to using the CsCl-based ICS described above, we also added 3 mM 4-AP, 100 µM DL-AP5, 20 µM CNQX, 100 µM CGP 35348, 100 µM CdCl$_2$ and 1 µM TTX to the bath solution to minimize the baseline noise and contribution from receptors other than GABA$_A$ receptors.

Two-photon laser-scanning microscopy

Two-photon imaging was conducted on a custom-built random scanning two-photon microscope [23]. An 840-nm femtosecond laser beam (pulse width of approximately 140 fs and repetitive rate of 80 MHz) was generated by a mode-locked Ti:sapphire laser (Chameleon Vision II, Coherent) and directed into a custom-made scanner head. A pair of perpendicular acousto-optic deflectors (AODs, DTSXY-400, AA optoelectronic, France) was employed for random-access scanning. The laser beam was then relayed through a dichroic mirror (DM665) into an upright microscope (BX61WI, Olympus) equipped with a 40 × water-immersion objective. The average laser power on the sample was generally 10–20 mW. Emitted green and red fluorescence were simultaneously collected by photomultiplier tubes (H7422-40, Hamamatsu). Imaging was controlled by a LabVIEW-based program on a PC with a PCI-6259 card (National Instruments, NI, USA) for communications and a PCI-6111 card (NI) for data acquisition.

For two-photon imaging, neurons were patched with the normal ICS without EGTA but with 200 µM Oregon Green Bapta-1 (OGB-1) and 50 µM Alexa Fluor 594. Ca^{2+} transients induced by APs were monitored at an acquisition rate of approximately 1 kHz in most cases, and represented as average (10 traces, 100-points moving average) time courses of $\Delta F/F$. To synchronize the imaging and patch clamp recording, a 5-V TTL pulse was sent from the MultiClamp 700B amplifier to the PCI-6259 card.

To examine the role of axonal GABA$_A$ receptors in regulating AP-induced Ca^{2+} transients, GABA was applied through ionto-phoresis using sharp electrodes. For visualizing the pipette tip and estimating the distance between the tip and the axon trunk, we also added 50 µM Alexa Fluor 594 to the pipette solution.

DAB staining

After recording, slices were transferred to 4% paraformaldehyde (PFA) in 0.1 M PB and kept in this fixative overnight. DAB staining was performed for visualization of the morphology of recorded neurons and measurement of the axon length.

Statistical analysis

Values are presented as the mean ± s.e.m. Excel (Microsoft) and OriginPro 8 (OriginLab Corporation) were used for statistical analysis. Student's t-test was used for statistic examination. Differences were considered to be statistically significant with $P < 0.05$.

Results

GABA$_A$ receptors are located in axon blebs and trunks

Previous studies have revealed the presence of GABA receptors at specific locations of the axon, including presynaptic terminals and the AIS [15,24]. To examine whether these receptors are also expressed at the main axon trunk of layer –5 pyramidal neurons in prefrontal cortex, we performed whole-cell recordings from axon blebs, the resealed cut ends of axons formed during slicing, and applied GABA locally to the axon via iontophoresis using sharp electrodes (Figure 1A).

Because GABA is positively charged at pH 3.6, we applied a retention current of –10 nA to prevent passive leakage of GABA but extruded GABA by delivering positive current pulses (200 nA, 2–5 ms in duration). These pulses could evoke an outward current at the axon bleb recorded with a low-Cl$^-$ pipette solution (7 mM [Cl$^-$]$_i$, holding potential: –50 mV). In contrast, no response could be observed when we applied negative current pulses (Figure 1A, inset). We next measured the diffusion distance of GABA by placing the iontophoresis electrode lateral to the recorded axon bleb with varying distance. The peak amplitude of GABA-induced currents (I$_{GABA}$) decreased progressively with increasing distance between the bleb and the tip of iontophoresis electrode. For 5-ms pulses (200 nA), GABA responses could hardly be detected if the distance was greater than 25 µm (Figure 1B). The retention current (–10 nA) applied to the iontophoresis electrode and the limited diffusion distance suggested that GABA did not spread widely and therefore did not activate dendritic receptors. However, GABA responses could be reliably obtained if the iontophoresis was performed near the axon trunk. As shown in Figure 1C, application of GABA at a lateral site *b* that was 25 µm away from the bleb could not induce any response; in contrast, at the site *c* (approximately 50 µm away from the bleb) we could observe GABA responses similar to those at the recorded bleb (site *a*). These results indicate the presence of GABA receptors at both the bleb and the main axon trunk. The filtering effect of the axon cable could be observed when we performed whole-cell recordings at the somata and applied GABA to the axon blebs with various distance from the somata (Figure S1). As expected, the rising slope of GABA-induced currents decreased but the decay time course increased with increasing distance between the soma and the axon bleb.

Application of GABA can activate both GABA$_A$ and GABA$_B$ receptors. Activation of GABA$_A$ receptors mainly induces a Cl$^-$ conductance, whereas activation of GABA$_B$ receptors induces a K$^+$ conductance. To examine the contribution of these receptors to axonal GABA responses, we measured the reversal potential of GABA-induced currents (E$_{GABA}$) by holding the V_m at different levels (–100 to –40 mV, Figure 2A). The average reversal potential was –78.2±0.8 mV (n = 12, corrected with a liquid junction potential of 15.4 mV), similar to the calculated equilibrium potential of Cl$^-$ (–78.3 mV) using the Nernst equation. Consistent with these results, bath application of 25 µM picrotoxin (PTX), a GABA$_A$ receptor antagonist, could abolish the GABA-induced
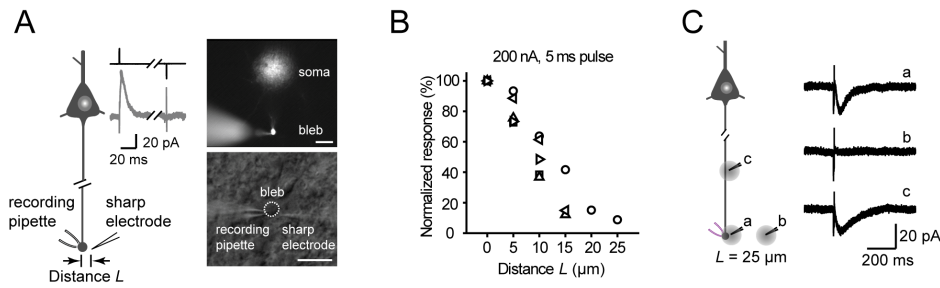
Figure 1. GABA receptors are located at axon bleb and trunk. A, Left, schematic diagram of bleb recording and GABA iontophoresis in a pyramidal neuron. Positive (but not negative) pulses could induce current responses. $V_{hold} = -50$ mV; iontophoresis pulses: 200 nA, 5 ms; retention current: −10 nA. Right, whole-cell recording from an axon bleb (top, fluorescence image; bottom, DIC image). Scale bar: 20 µm. The sharp electrode was used for GABA iontophoresis. Alexa Fluor 488 was added to the patch pipette solution so that the recording pipette was visible. B, Plot of the normalized GABA response as a function of the distance between the bleb and the tip of the iontophoresis electrode. Different symbols indicate different cells. The measurement of distance *L* is shown in the schematic diagram in panel A (indicated by arrows). C, GABA-induced responses could be observed when GABA was applied to the bleb (site *a*) or the main axon trunk (site *c*). The distance between sites *a* and *c* was approximately 50 µm, whereas that between *a* and *b* was approximately 25 µm. $V_{hold} = -80$ mV; iontophoresis pulses: 200 nA, 5 ms.
doi:10.1371/journal.pone.0100968.g001

current recorded at the axon bleb (reduced to 11.3±3.7% of control, n = 6, Figure 2B). These results indicate that GABA responses at the axon are mediated by GABA_A receptors.

We next applied baclofen, a GABA_B receptor agonist, to further address whether GABA_B receptors were expressed at the axon trunk. Consistent with previous findings [25], local puff application of 200 µM baclofen at the soma induced a current with a reversal potential of −102.1±1.1 mV (n = 13, corrected with a liquid junction potential of 15.4 mV. Figure 2C), which was close to the calculated equilibrium potential of K⁺ (−107.8 mV). However, we

observed no significant changes in the baseline currents (holding potential: −100 to −50 mV) after the application of baclofen to the axon bleb (Figure 2C). Consistent with these results, the GABA_A receptor antagonist PTX but not the GABA_B receptor antagonist CGP 35348 could block the currents evoked by iontophoresis of GABA at the axon (Figure 2D). Together, these results show that GABA_A but likely not GABA_B receptors (at least not GABA_B-coupled potassium channels) are expressed along the axon.

The GABA receptors at the AIS can be activated upon GABA release from the axo-axonic synapses [26,27]. Considering the lack
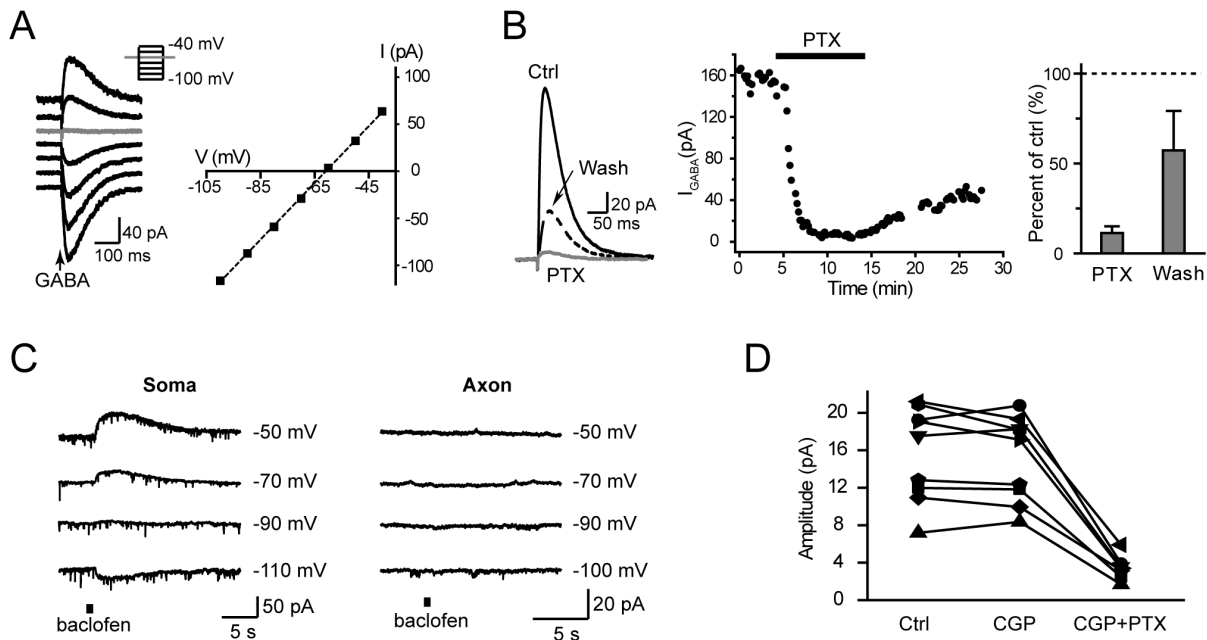
Figure 2. The presence of GABA_A (but likely not GABA_B) receptors in the axon. A, Reversal potential of GABA responses (I_GABA) in the axon bleb. Left, representative currents induced by GABA application at different holding potentials (from −100 to −40 mV). At −60 mV (near reversal potential), GABA application induced no obvious change in baseline current (gray). Right, I-V curve of the GABA-induced responses shown on the left. B, I_GABA could be blocked by GABA_A receptor blocker PTX. Left, example traces before (black), during (gray) and after (Wash, dashed line) the bath application of PTX (25 µM). $V_{hold} = -50$ mV, GABA was applied via iontophoresis. Middle, time course of the effect of PTX. Right, group data showing the change of I_GABA during (n = 6) and after (n = 3) PTX application. The dashed line indicates 100% of control. C, Left, currents evoked by puffing baclofen (200 µM), a GABA_B receptor agonist, to the soma (16 psi, 15 ms). Right, no response was observed when baclofen was applied to the axon trunk (16 psi, 20 ms). D, Group data showing that GABA-induced currents at the axon blebs could not be blocked by the GABA_B receptor antagonist CGP 35348 (100 µM); however, PTX could diminish these responses. Different symbols indicate different cells.
doi:10.1371/journal.pone.0100968.g002

of direct evidence of GABAergic synapses at the axon trunk, we speculated that these axonal GABA$_A$ receptors may be activated by ambient GABA. To exclude the contribution of somatodendritic GABA receptors, we performed the following experiments in isolated axon blebs that were disconnected from the soma but with axon segments attached (see the Methods section, Figure 3A). In the presence of the GABA$_A$ receptor agonist muscimol (5 µM), we observed an increase in outward holding current ($\Delta I = 14.8 \pm 4.3$ pA, n = 11; low-Cl$^-$ ICS) at a holding potential of 10 mV. Again, 100 µM PTX could block this effect (Figure 3B). At a holding potential of −70 mV, we also observed a decrease in the inward holding current after the application of PTX ($\Delta I = −5.8 \pm 2.3$ pA, n = 6; CsCl ICS), even without the presence of muscimol (Figure 3C). These results suggest that ambient GABA (mimicked by a low concentration of muscimol) can activate axonal GABA$_A$ receptors.

Next, we investigated the average conductance γ and the open time constant τ of these axonal receptors by using noise analysis (see the Methods section). Membrane current responses to 5 µM muscimol were recorded at isolated blebs, and the variance σ_i^2 and cut-off frequency f_c could be then obtained (Figure 3D, E, F). In most cases, the power spectral density plots of membrane current fluctuations could be well fitted by a double Lorentzian function and yielded two f_c values and consequently two τ values. The γ, τ_1, and τ_2 values for axonal GABA$_A$ receptors activated by 5 µM muscimol were 23.4 ± 1.6 pS, 45.7 ± 3.0 ms and 8.2 ± 0.9 ms, respectively (n = 10). All values were quite similar to those obtained from somatic GABA$_A$ receptors by using nucleated patch recording (23.5 ± 1.2 pS, 45.1 ± 6.0 ms and 7.0 ± 0.6 ms, n = 9). These results show no significant difference in single-channel properties between axonal and somatic GABA$_A$ upon activation by a low concentration of muscimol.

Axonal GABA$_A$ receptors hyperpolarize the axon

Activation of GABA$_A$ receptors in the somatodendritic compartments hyperpolarizes the V_m and thus inhibits and structures neuronal activities [14]. However, different results were observed for axonal GABA$_A$ receptors in different subcellular locations and brain regions, such as the AIS of hippocampal [17] and neocortical pyramidal neurons [15], the axon trunk of cerebellar granule cells [19] and axon terminals of hippocampal mossy fibers [18].

In our experiment, we used noninvasive gramicidin perforated patch recording to examine the reversal potential of GABA responses (E$_{GABA}$) under physiological conditions. Because gramicidin-formed holes are not permeable to Cl$^-$, the intracellular Cl$^-$ gradient is not perturbed during this type of perforated patch recording. Because we added Alexa Fluor 488 to the pipette solution, rupture of the membrane would result in the presence of fluorescence in the recorded cell or bleb (Figure 4A). In these experiments, we used a high-Cl$^-$ pipette solution, and rupture of the membrane would also lead to a dramatic change in E$_{GABA}$ (Figure 4B). These results revealed that E$_{GABA}$ at the distal axonal bleb (>100 µm apart from the soma) was −67.3 ± 1.5 mV (n = 14), significantly more positive than that at the soma (−79.0 ± 2.3 mV, n = 13. p<0.01, two-sample t-test). However, both values were more negative (hyperpolarizing) than the respective local resting V_m (RMP) (Figure 4C). In distal axons, the RMP and E$_{GABA}$ were −61.0 ± 2.1 mV and −67.2 ± 1.6 mV (n = 13. P = 0.02, paired t-test), respectively. Similar results were obtained when we
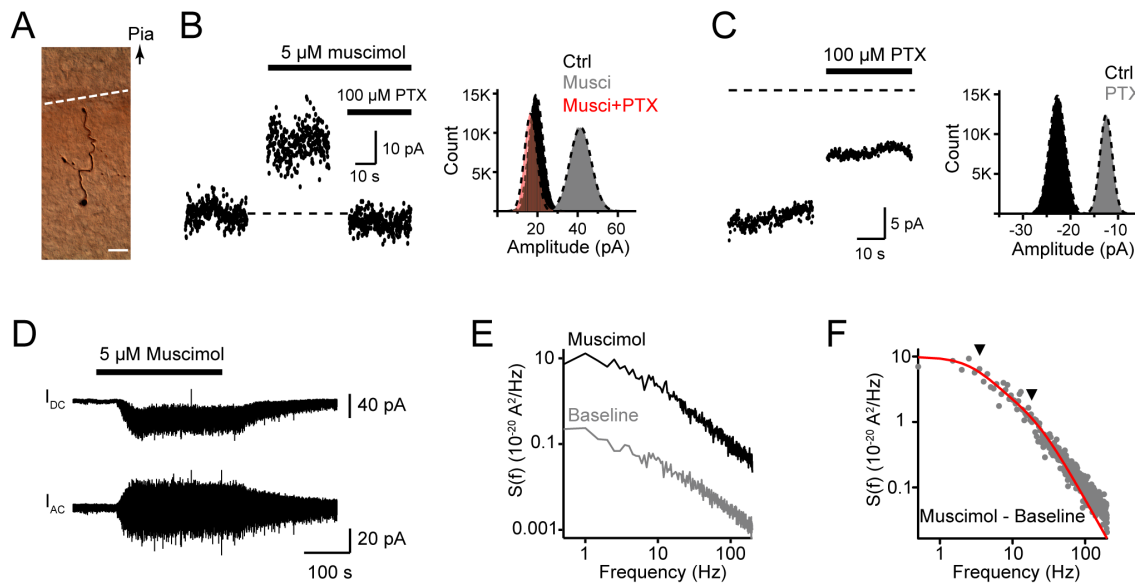
Figure 3. Properties of axonal GABA$_A$ receptors. A, DAB staining of an isolated axon bleb. The axon bleb was mechanically isolated from the main axon trunk before recording (see the Methods section). Arrow indicates the direction of the pia. Dashed line indicates the cut. Scale bar: 20 µm. B, Left, an example trace showing an increase in outward holding current after bath application of 5 µM muscimol (V$_{hold}$ = 10 mV) and the blockade of this increase by 100 µM PTX. The dashed line indicates the baseline holding current. The mean values of I$_{hold}$ for "Ctrl", "Musci" and "Musci + PTX" group were 19.8, 41.4 and 16.9 pA, respectively. Right, histograms of the membrane currents shown on the left. The best-fit curves (dashed lines) were single Gaussian distributions. Axon blebs were recorded with patch pipettes filled with a low-Cl$^-$ ICS (7 mM [Cl$^-$]$_i$). C, Left, an example trace showing a decrease in inward holding current after bath application of 100 µM PTX (V$_{hold}$ = −70 mV). The mean values of I$_{hold}$ for "Ctrl" and "PTX" group were −22.8 and −12.5 pA, respectively. Right, histograms of the membrane currents shown on the left. Patch pipettes were filled with CsCl-based ICS (149 mM [Cl$^-$]$_i$). D, Current traces recorded in an isolated bleb. V$_{hold}$ = −60 mV, CsCl-based ICS was used. Top, the actual current response; bottom, current trace with DC Remove. E, Power spectral density plots of membrane current fluctuations in control and muscimol-treated conditions (same data as in D). F, Subtraction of the power spectral density in the control from that with muscimol treatment (same data from D and E). The red line was the fitting curve of double Lorentzian functions. Cut-off frequencies (f_c) of the two components (arrowheads) were 3.5 and 18.1 Hz.
doi:10.1371/journal.pone.0100968.g003
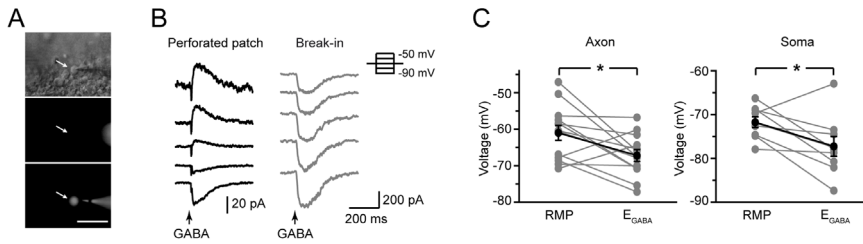
Figure 4. Reversal potential of GABA responses (E$_{GABA}$) is more negative than the local RMP. A, Gramicidin perforated patch recording from an axon bleb. Arrow indicates the recorded bleb. Top, DIC image of the recording; middle, fluorescence image (unlabeled bleb); bottom, fluorescence image (labeled bleb, indicating rupture of patch membrane). Scale bar: 50 μm. B, Example traces showing GABA responses at different holding potentials (from –90 to –50 mV) before (black) and after the break-in (membrane rupture, gray). C, Comparison of E$_{GABA}$ and RMP. Note that E$_{GABA}$ at both the soma and the distal axon bleb were more hyperpolarized than their local RMP. *, P<0.05, paired t-test.
doi:10.1371/journal.pone.0100968.g004

performed perforated patch recording at the soma (RMP: –71.7±1.2 mV; E$_{GABA}$: –77.3±2.3 mV, n = 9. P = 0.03, paired t-test). Together, these results suggest that GABA functions as an inhibitory transmitter (hyperpolarizing the axon) at V_m levels more positive than the RMP.

Axonal GABA$_A$ receptors regulate AP waveform

We next investigate the role of axonal GABA$_A$ receptors in regulating orthodromically propagating APs along the axon. APs were evoked by extracellular stimulation with a concentric electrode and AP waveforms were monitored at the bleb. Three types of intracellular solutions (ICS) were employed in this experiment, they were low-Cl$^-$ ICS (7 mM [Cl$^-$]$_i$), modified ICS (20 mM [Cl$^-$]$_i$) and high-Cl$^-$ ICS (75 mM [Cl$^-$]$_i$), respectively.

Based on the results that activation of axonal GABA$_A$ receptors may hyperpolarize the axon, we speculated that the [Cl$^-$]$_i$ in the distal axon trunk should be low. We therefore used the low-Cl$^-$ ICS first and found that the waveform of the evoked AP could be modulated by GABA applied to the axon bleb (Figure 5A). When the V_m was maintained at approximately –50 mV in current-clamp mode, GABA application at the bleb could cause hyperpolarization (–2.4±0.6 mV, ranging from –1.0 to –5.5 mV, n = 7). Although the amplitude showed no significant change (99.0±2.8% of control, P = 0.81, 41.3 vs. 41.0 mV, n = 7), the half-widths of APs were significantly decreased to 91.4±3.2% (P = 0.04, 1.4 vs. 1.3 ms, n = 7) of the control (black plots, Figure 5B., paired t-test). Then, we clamped the V_m of the bleb to a more hyperpolarized level at approximately –65 mV, application of GABA to the axon caused depolarization (3.4±1.1 mV, ranging from 1.0 to 8.0 mV, n = 6). Interestingly, both the AP amplitude and the AP half-width were significantly reduced (gray, Figure 5B). These values were decreased to 91.5±2.6% (P = 0.03, 78.9 vs. 72.1 mV) and 92.6±2.5% (P = 0.04, paired t-test, 0.94 vs. 0.87 ms) of the control, respectively. Together, our results indicate that GABA application at the axon reduces AP duration whether it hyperpolarizes or depolarizes the V_m, presumably resulting from a shunting effect of the GABA-induced conductance.

It has been reported that axo-axonal chandelier cells innervate the AIS of postsynaptic pyramidal cells and induce depolarizing responses, due to a high [Cl$^-$]$_i$ at this strategic location (AP initiation site). Therefore, we increased the [Cl$^-$]$_i$ from 7 to 20 mM (modified ICS) to mimic conditions of relatively high [Cl$^-$]$_i$ at AIS, depolarizing E$_{GABA}$ to –48.0±0.5 mV (n = 19, corrected with a liquid junction potential of 14 mV). Although GABA iontophoresis at the bleb caused a larger depolarization (8.0±0.9 mV, ranging from 5.3 to 13.6 mV, n = 8), the amplitude and the half-width of APs decreased to 77.9±2.9% and

93.5±0.9% of control (P<0.001), respectively (Figure 5C). Bath application of PTX (25–50 μM) could block these GABA-induced depolarization and AP waveform changes (Figure 5D). Again, application of baclofen at the bleb caused no significant change in either the amplitude (P = 0.18) or the half-width (P = 0.22, paired t-test. n = 5) of AP waveforms. These results further support the shunting effect of GABA$_A$ receptors on AP waveform at the axon.

Further increasing the [Cl$^-$]$_i$ in the pipette solution to 75 mM (high-Cl$^-$ ICS; reversal potential: –10.8±0.6 mV, corrected with a liquid junction potential of 9 mV, n = 17) produced larger depolarization and even facilitated the generation of APs. As shown in Figure 5E, GABA iontophoresis could evoke a large depolarization and sometimes even generate APs (arrow). Again, this GABA response also showed an inhibitory effect on the AP waveform when the orthodromic AP was evoked during GABA application (asterisk, Figure 5E). The dramatic decrease in AP amplitude resulted from an increase in membrane conductance (shunting effect) and a decrease in Na$^+$ channel availability (depolarization-induced inactivation). Interestingly, GABA-evoked depolarization could not promote the initiation of APs even when the strength of extracellular stimulation was very close to the threshold (data not shown).

Together, these results indicate that the waveforms of orthodromically propagating APs at the axon can be modulated by axonal GABA$_A$ receptors. Activation of these receptors mainly showed a shunting effect on AP waveforms regardless of the polarity of GABA-induced V_m changes.

Propagation of GABA-induced hyperpolarization along the axon

The shunting effect induced by increased conductance may occur only at the location where the receptors were activated; however, it remains unclear whether GABA-induced V_m changes at remote locations could influence AP initiation and propagation. To address this question, we performed simultaneous recordings from the soma and the bleb with low-Cl$^-$ ICS, and then applied GABA through iontophoresis to the axon trunk to investigate its role in regulating AP generation (Figure 6A).

GABA application to the axon trunk could result in V_m hyperpolarization or depolarization (with low-Cl$^-$ ICS), depending on the V_m when GABA was applied. These V_m changes could propagate to the soma and the recorded bleb (Figure 6B). Because E$_{GABA}$ at the axon was more negative than the RMP (Figure 4), GABA receptor activation could hyperpolarize the axon. Given that the voltage fluctuations could propagate along the main axon with a length constant of hundreds of micrometers [2], V_m hyperpolarization could spread along the axon trunk and even reach the presynaptic terminals. Activation of axonal GABA
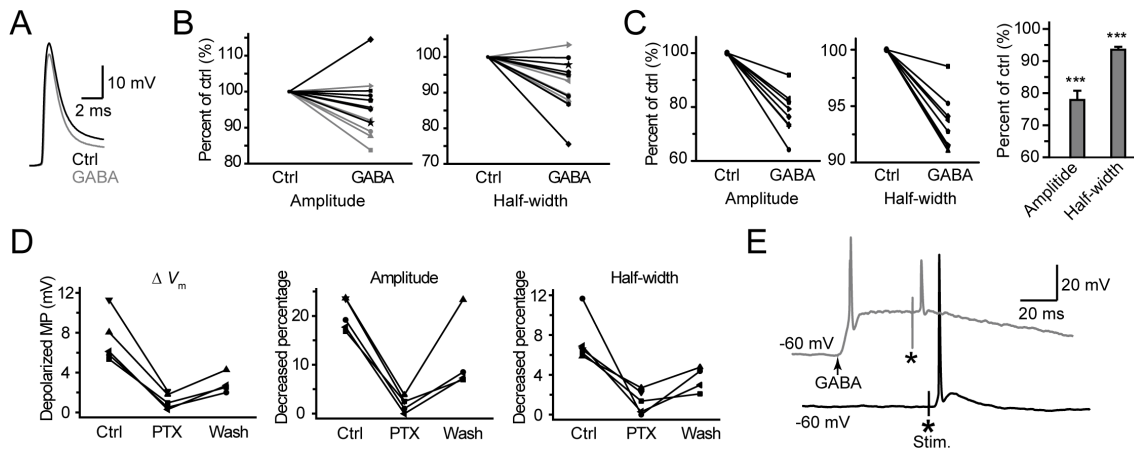
Figure 5. Activation of axonal GABA_A receptors shapes the AP waveform. A, Example traces showing the change in AP waveform after GABA iontophoresis to the axon bleb. V_m change was −3.9 mV in this bleb. The amplitude and the half-width of APs decreased to 95.6% and 86.8% of the control, respectively. B, Group data showing that activation of axonal GABA_A receptors shaped AP waveforms by regulating the amplitude and the half-width. Note that the recordings were performed under current-clamp and that the V_m could be manipulated by DC current injection. Black, GABA responses were hyperpolarizing; gray, depolarizing. The blebs were recorded with low-Cl⁻ ICS (7 mM [Cl⁻]_i). C, Increasing [Cl⁻]_i depolarized the V_m but still showed a shunting effect on AP waveforms. Amplitude and half-width were significantly reduced. Modified ICS (20 mM [Cl⁻]_i) was used for these recordings. ***, P<0.001, paired t-test. D, Bath application of PTX could block the GABA-induced V_m depolarization and its shunting effect on AP waveform. Modified ICS was used. E, Example traces showing that GABA application caused a shunting effect on APs evoked by electric shocks (asterisks), although GABA itself could evoke an AP (arrow). High-Cl⁻ ICS (75 mM [Cl⁻]_i) was used here.
doi:10.1371/journal.pone.0100968.g005

receptors at the main trunk could increase the amplitude (by 3.2±0.7%, n = 7. P<0.01) but did not produce a significant change in AP half-width (decreased by 2.2±1.4%, n = 7. P = 0.15). This phenomenon was similar to the AP waveform changes caused by hyperpolarization induced by negative current injection (amplitude: by 4.7±2.0%, P = 0.04; half-width: by 3.4±0.7%, P = 0.04; n = 5. Figure 6C). Therefore, activation of remote axonal GABA receptors could also regulate the waveform of propagating APs by hyperpolarizing the membrane potential.

We next injected step currents (100–500 pA, 500 ms) at the soma to evoke a train of APs, and corresponding APs could be observed at the bleb. As shown in Figure 6D, we observed a failure of AP initiation for weak somatic stimulation (gray, 100–200 pA, n = 3) and a decrease in firing frequency for strong stimulation (black, 400–500 pA, n = 5) when GABA was applied to the distal axon trunk (>100 μm apart from the soma). In contrast, when GABA was delivered at the AIS, substantial hyperpolarization (recording with pipettes filled with Low-Cl⁻ ICS) and failure of AP initiation could be observed during both weak and strong current stimulation (200 and 400 pA, n = 7), presumably due to the strategic function of AIS for AP initiation. Iontophoresis of GABA to the main trunk could cause a decrease in the instantaneous firing frequency at the distal axon bleb (Figure 6E). The mean frequency of APs evoked by step current injection (400–500 pA) dropped from 24.7±2.0 to 20.1±2.3 Hz (P<0.01, paired t-test. n = 5) immediately after GABA application (Figure 6E). These results indicate a role for axonal GABA_A receptors in regulating AP generation and firing frequency.

Regulation of AP-induced Ca²⁺ transients by axonal GABA_A receptors

Previous studies revealed that changes in AP waveforms could regulate the amount of Ca²⁺ entry, leading to changes in neurotransmitter release [28,29]. We therefore speculated that AP waveform changes induced by the activation of axonal GABA_A receptors could also regulate intracellular Ca²⁺ levels in the axon and the consequent neurotransmitter release.

We performed two-photon Ca²⁺ imaging to investigate whether AP-induced Ca²⁺ transients at the axon were subject to modulation by iontophoresis of GABA. As shown in Figure 7A, a layer −5 pyramidal neuron was filled with Alexa Fluor 594 (50 μM) and the Ca²⁺ indicator OGB-1 (200 μM) through the whole-cell patch pipette. Several regions of interest (ROIs) were selected for optical recording. We observed a decrease in Ca²⁺ transients in the axon (ROI 1 and 2, Figure 7A) after GABA application; however, the Ca²⁺ signals at the soma, which was remote from the GABA iontophoresis site, were not affected. In this particular cell, the distance between the iontophoresis site and ROI 1, ROI 2 and the soma were 36, 21 and 127 μm, respectively. The direction of bath flow was always from the soma to the axon, and the GABA application site was defined as 0. The distances between the application site and downstream or upstream ROIs were shown as positive or negative values, respectively. Group data from 13 cells showed that local GABA application decreased the Ca²⁺ transients induced by single APs by 14.1±1.4% at the axonal segments (ranging from −39 to 55 μm, n = 68 ROIs) that were close to the iontophoresis site (Figure 7B); no significant change was observed in 9 ROIs with distances longer than −40 μm. In contrast, Ca²⁺ transients at the soma showed no significant decrease (P = 0.84) after GABA application at a distance>100 μm from the soma. Significant reduction (P<0.01) in Ca²⁺ transients was detected only when the distance between the soma and GABA application site was less than 100 μm (Figure 7B).

Similarly, axonal Ca²⁺ transients evoked by a train of 3 APs at 100 Hz were also significantly decreased by local GABA application (by 10.9±1.2%, axonal segments ranging from −59 to 59 μm, n = 61 ROIs of 9 cells. Figure 7C); no significant change was observed in 7 ROIs with distance greater than −60 μm. Bath application of PTX could block the GABA-induced decrease in Ca²⁺ transients evoked by either single APs (n = 11 ROIs of 3 cells) or bursts of 3 APs (n = 25 ROIs of 6 cells), indicating a role for axonal GABA_A receptors in modulating local Ca²⁺ signals (Figure 7D).
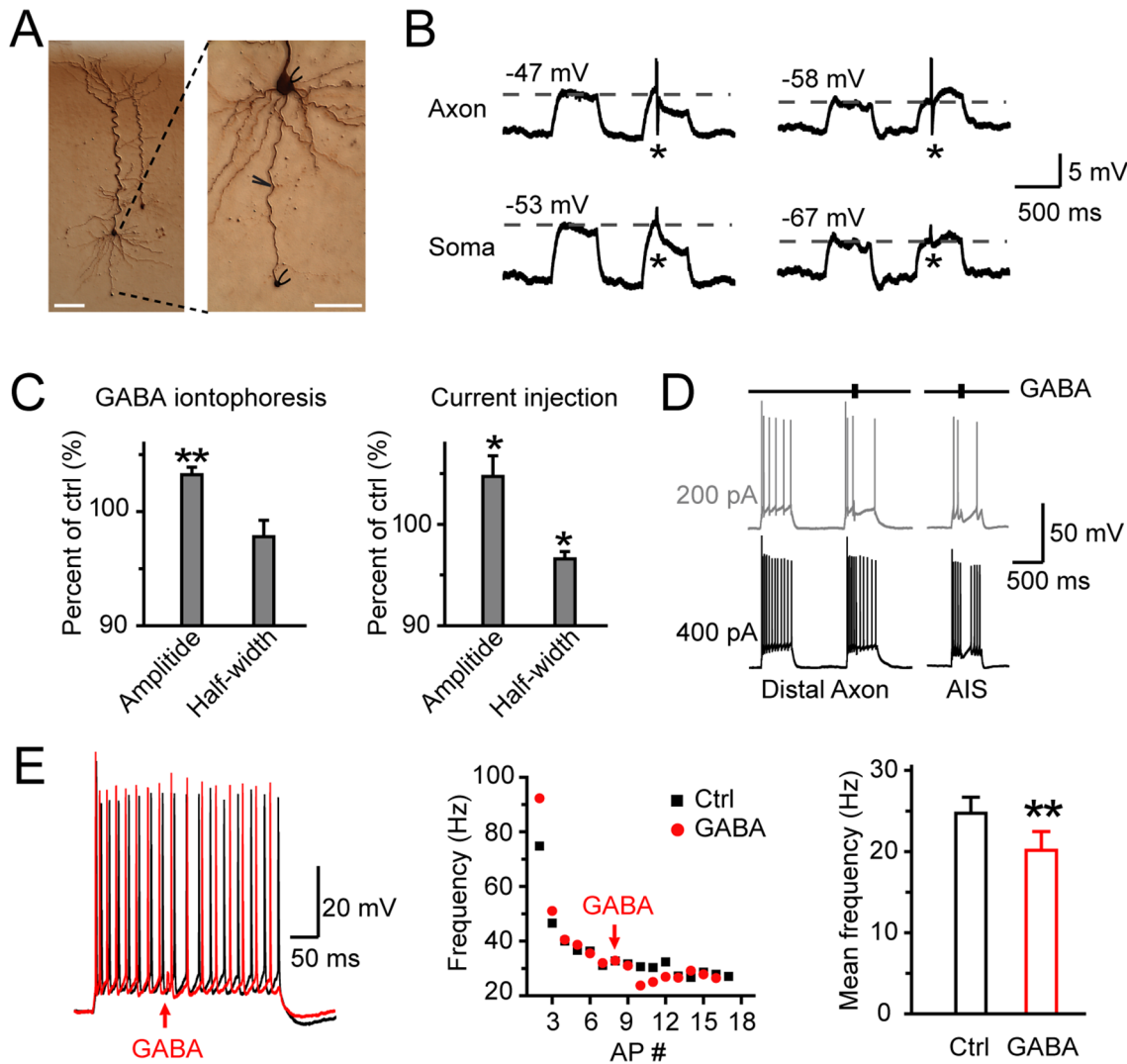
Figure 6. Propagation of GABA-induced hyperpolarization at the axon regulates AP generation. A, DAB staining of recorded neurons. Simultaneous recording from the soma and axon bleb were performed in a pyramidal neuron (left), and GABA was applied to the axon trunk (right). The axon length was 239 μm in this case. The distance between the iontophoresis site and the soma was 117 μm. Scale bar: 100 μm (left); 50 μm (right). B, The sign of the effect of GABA (hyperpolarization or depolarization) depended on the V_m. Top, traces were taken from the bleb. Bottom, traces were the corresponding responses at the soma. The V_m was clamped through somatic DC current injection. Asterisk indicates application of GABA to the main trunk. C, Left, application of GABA to the axon increased the amplitude but decreased the half-width of propagating APs. GABA iontophoresis hyperpolarized the V_m by 2.3±0.4 mV (n = 7). Right, similar results were obtained when V_m was hyperpolarized by 2.8±0.3 mV (n = 5) through DC current injection. *, P<0.05; **, P<0.01, paired t-test. D, Example traces showing activation of axonal GABA_A receptors reduced firing probability and frequency. The distances between the iontophoresis site and the soma were 100 μm (distal axon) and 18 μm (AIS). E, Left, repetitive firing recorded at an axon bleb induced by 400 pA DC current injection at the soma before (black) and after (red) GABA application to the axon trunk. The arrow indicates GABA iontophoresis. Middle, instantaneous firing frequency of APs decreased after GABA application (same data as shown in the left). Right, group data showing a decrease in the mean frequency of APs after GABA iontophoresis at the axon trunk. **, P<0.01, paired t-test. Low-Cl⁻ ICS was used in these experiments.
doi:10.1371/journal.pone.0100968.g006

Discussion

In this study, we found that GABA_A receptors were expressed at the main axon trunks of layer – 5 pyramidal neurons and that activation of these receptors mainly hyperpolarized local V_m under physiological conditions. Importantly, we also show that waveforms of propagating APs could be shaped by either GABA-induced shunting or hyperpolarizing effects. Consistent with these results, AP-induced Ca^{2+} transients were substantially reduced by GABA application to the axon trunk, suggesting an important role for axonal GABA_A receptors in regulating the output signal of pyramidal neurons.

Previous studies revealed the expression of GABA_A receptors at presynaptic axons [24,30,31,32,33,34]. Those axonal GABA_A receptors have been described as localizing in various brain regions including the spinal cord, brainstem, the cerebellum, the hippocampus and the cortex. Due to difficulties in recording from thin axons with diameter less than 1 μm [35], the properties and function of axonal GABA receptors have received much less attention than somatodendritic receptors. At the axon, GABA receptors distributed in some special axonal compartments such as the AIS (thicker than the main axon) and axon terminals (e.g., hippocampal mossy fiber boutons and midbrain calyx of Held)
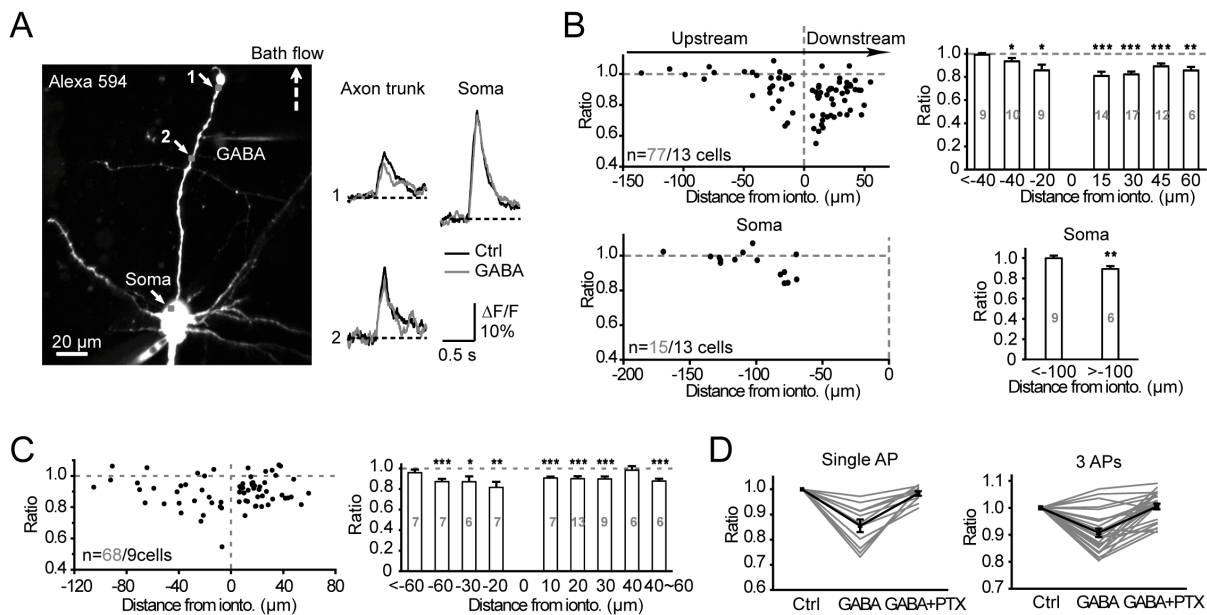
Figure 7. Activation of axonal GABA_A receptors decreases AP-induced Ca^{2+} transients. A, Left, projection of 2-photon fluorescence images of a recorded pyramidal neuron filled with Alexa Fluor 594 (50 µM) and OGB-1 (200 µM). The dashed arrow indicates the direction of bath flow. Right, iontophoresis of GABA at the axon trunk (labeled by "GABA" in the left image) decreased Ca^{2+} transients evoked by single APs at nearby locations (ROI 1 and 2) but showed no effect on somatic transients. B, Group data showing the effect of GABA on single-AP-triggered Ca^{2+} transients. The results are presented as the ratio of the Ca^{2+} signal amplitude for "GABA" to "Ctrl." Top, data collected from the axon trunk (n = 13 axons). Bottom, data collected from the soma. The site for GABA iontophoresis was defined as 0. If the ROI was located downstream from the iontophoresis site, the sign of the distance was positive; otherwise it was assigned a negative sign. *, P<0.05; **, P<0.01; ***, P<0.001, paired t-test. C, Group data showing the effect of GABA on Ca^{2+} transients induced by 3 APs (100 Hz). Data were collected from the axon trunk (n = 9 axons). D, PTX blocked GABA-induced decrease in Ca^{2+} transients. Gray, individual cells; black, average data.
doi:10.1371/journal.pone.0100968.g007

have been studied. In this study, by using the bleb recording method [2], we could directly examine the properties of ion channels and transmitter receptors located in the axon trunk. A previous study using high-Cl$^-$ ICS (approximately 140 mM) revealed that pairing GABA iontophoresis with antidromic axonal stimulation could substantially decrease spike failures [36]. Here, we employed multiple types of ICS with varying Cl$^-$ concentrations and showed the existence of GABA_A receptors at the distal axon of layer –5 pyramidal neuron in prefrontal cortex. In addition, both that previous study and our findings revealed no presence of glutamate receptors at the axon, which is different from the pattern found in CA3 pyramidal neurons [7].

There is still debate regarding whether activation of axonal GABA_A receptors induces hyperpolarization or depolarization. To address this question, one must know the difference between the RMP and E_GABA at the axon. With a variety of noninvasive recording methods performed on axon including the AIS [15,37], axon trunk [19] and presynaptic terminals [18], previous studies showed that axonal E_GABA was more depolarized than RMP so GABA responses increased neuron excitability. However, the unitary field potential recordings performed on hippocampal CA1 pyramidal cells suggested that activation of axo-axonic synapses induces hyperpolarizing responses [17]. In our experiments, we found that E_GABA in the distal axon trunk (beyond the AIS) is more hyperpolarized than the local RMP (–67 vs. –61 mV). Unlike some of the reports mentioned above, our findings suggest that GABA can induce hyperpolarization at distal axonal segments. Because E_GABA is mainly determined by [Cl$^-$]_i, the conflicting results could be explained by different [Cl$^-$]_i. A higher [Cl$^-$]_i can result in a more depolarized E_GABA. The [Cl$^-$]_i varies across developmental stages and brain regions. Even within the same

brain region, it has also been reported that the response induced by GABA can be cell-type specific [38,39,40]. At one extreme, the GABA-mediated response in the suprachiasmatic nucleus is excitatory during the day but inhibitory during the night [41]. Various cation-chloride co-transporters play pivotal roles in maintaining intracellular chloride homeostasis [42,43]. The Na$^+$-K$^+$-2Cl$^-$ co-transporters (NKCCs) account for Cl$^-$ accumulation, whereas K$^+$-2Cl$^-$ co-transporters (KCCs) account for Cl$^-$ extrusion. In retina, the expression pattern of cation-chloride co-transporters shows specificity in cell type and subcellular locations [44]. In cortex, the co-operation of NKCC1 and KCC2 results in a relatively high [Cl$^-$]_i in AIS and therefore depolarizes E_GABA [15,37]. The distribution pattern and function of these co-transporters at the axon trunk remains to be further examined.

However, hyperpolarization and depolarization cannot simply be considered as inhibitory and excitatory, respectively. Under some circumstances, presynaptic depolarization mediated by axonal GABA_A receptors results in activation of voltage-gated Ca^{2+} channels, even causing AP initiation [45]. In other cases, presynaptic inhibition occurs because of inactivation of Na$^+$ and/or Ca^{2+} channels. GABA-induced depolarization may reduce the amplitude of APs and cause a decrease in Ca^{2+} influx [24,46]. Furthermore, opening of GABA_A receptor channels will introduce a leaky conductance during generation of APs and propagation of postsynaptic potentials whether the GABA response is depolarizing or hyperpolarizing [47,48]. The actual effect of GABA also depends on the precision of the timing and location [49,50]. Therefore, the shunting inhibition together with V_m changes must be taken into account in analyses of the effect of GABA. In our study, GABA-mediated inhibition is associated with both hyperpolarization and shunting under physiological conditions. By

increasing the [Cl$^-$]$_i$ to a high level (75 mM), GABA application itself can evoke APs if the depolarizing response overcomes the shunting conductance and reaches the threshold for AP generation (Fig. 5E).

The concentration of GABA in the synaptic cleft can reach a millimolar level [51,52] and the ambient GABA concentration varies from nanomolar to a few micromolar [53,54]. GABA$_A$ receptors located in the distal axon trunk can be activated by a low concentration of muscimol (5 μM). Additionally, the change of holding current in the presence of PTX was consistent with previous findings [55,56]. These results suggest that axonal GABA$_A$ receptors have high affinity to GABA and can be tonically activated. Before entering the white matter, the axon segments (approximately 400 μm in length) of layer –5 pyramidal neurons in prefrontal cortex are not myelinated [57]. These axon segments may be subcellular candidates for the modulation of neuronal output signals. We have recently shown that at these unmyelinated axons K$^+$ currents and AP waveforms are subject to dopaminergic modulation [58]. At the direct activation site, the GABA-induced shunting effect can regulate the AP waveform by decreasing the amplitude and the half-width. Beyond this site, GABA-induced hyperpolarization can propagate for hundreds of micrometers and decrease the AP width in contrast to the action of subthreshold depolarization [2,59]. Consistent with previous findings showing a linear dependence of Ca^{2+} influx on AP half-width [28,60], our Ca^{2+} imaging results show a decrease in AP-induced Ca^{2+} transients after GABA application to the axon.

In summary, we show the existence of GABA$_A$ receptors at the axon trunk of cortical pyramidal neurons. Activation of these receptors shortens propagating APs and decrease AP-induced Ca^{2+} entry by shunting and/or hyperpolarization. GABA-induced changes in axonal AP waveforms may represent a new mechanism for GABAergic modulation of synaptic transmission in the cortex.

Supporting Information

Figure S1 Filtering effect of the axon cable on GABA-induced currents. A, Example recording at the soma with GABA iontophoresis at the axon bleb. The red line indicates the linear fit of the rising phase, the rising slope can be derived from this fit. The red dashed line is an exponential fit of the decay phase, the decay time course can be then obtained. In this experiment, whole-cell recording was achieved at the soma with low-Cl$^-$ ICS (V$_{hold}$ = –40 mV) while GABA was applied at the axon bleb via iontophoresis (200 nA, 5 ms). B, Left, a plot of the rising slope of the GABA-induced currents as a function of the distance between the bleb and the soma (distance L, n = 29). Right, the pooled data shown on the left were divided into three subgroups according to the distance L. The rising slope of each group was 6.0±0.7 (n = 6), 2.0±0.4 (n = 15), 0.9±0.3 (n = 8), respectively. C, Left, a plot of the decay time course as a function of the distance L (n = 29). Right, the decay time course of each subgroup was 168.4±47.6 (n = 6), 216.6±34.1 (n = 15), 305.8±88.2 (n = 8), respectively.
(TIF)

Author Contributions

Conceived and designed the experiments: SZ YS. Performed the experiments: YX YZ. Analyzed the data: YX YZ MY. Contributed reagents/materials/analysis tools: YX YZ MY. Contributed to the writing of the manuscript: YX YS.

References

1. Alle H, Geiger JR (2006) Combined analog and action potential coding in hippocampal mossy fibers. Science 311: 1290–1293.
2. Shu Y, Hasenstaub A, Duque A, Yu Y, McCormick DA (2006) Modulation of intracortical synaptic potentials by presynaptic somatic membrane potential. Nature 441: 761–765.
3. Christie JM, Jahr CE (2008) Dendritic NMDA receptors activate axonal calcium channels. Neuron 60: 298–307.
4. Kole MH, Letzkus JJ, Stuart GJ (2007) Axon initial segment Kv1 channels control axonal action potential waveform and synaptic efficacy. Neuron 55: 633–647.
5. Shu Y, Yu Y, Yang J, McCormick DA (2007) Selective control of cortical axonal spikes by a slowly inactivating K+ current. Proc Natl Acad Sci U S A 104: 11453–11458.
6. Turecek R, Trussell LO (2001) Presynaptic glycine receptors enhance transmitter release at a mammalian central synapse. Nature 411: 587–590.
7. Sasaki T, Matsuki N, Ikegaya Y (2011) Action-potential modulation during axonal conduction. Science 331: 599–601.
8. Engelman HS, MacDermott AB (2004) Presynaptic ionotropic receptors and control of transmitter release. Nat Rev Neurosci 5: 135–145.
9. Zucker RS, Regehr WG (2002) Short-term synaptic plasticity. Annu Rev Physiol 64: 355–405.
10. Moss SJ, Smart TG (2001) Constructing inhibitory synapses. Nat Rev Neurosci 2: 240–250.
11. Farrant M, Kaila K (2007) The cellular, molecular and ionic basis of GABA(A) receptor signalling. Prog Brain Res 160: 59–87.
12. Miles R, Toth K, Gulyas AI, Hajos N, Freund TF (1996) Differences between somatic and dendritic inhibition in the hippocampus. Neuron 16: 815–823.
13. Pouille F, Scanziani M (2001) Enforcement of temporal fidelity in pyramidal cells by somatic feed-forward inhibition. Science 293: 1159–1163.
14. Somogyi P, Klausberger T (2005) Defined types of cortical interneurone structure space and spike timing in the hippocampus. J Physiol 562: 9–26.
15. Szabadics J, Varga C, Molnar G, Olah S, Barzo P, et al. (2006) Excitatory effect of GABAergic axo-axonic cells in cortical microcircuits. Science 311: 233–235.
16. Ben-Ari Y (2002) Excitatory actions of gaba during development: the nature of the nurture. Nat Rev Neurosci 3: 728–739.
17. Glickfeld LL, Roberts JD, Somogyi P, Scanziani M (2009) Interneurons hyperpolarize pyramidal cells along their entire somatodendritic axis. Nat Neurosci 12: 21–23.
18. Ruiz A, Campanac E, Scott RS, Rusakov DA, Kullmann DM (2010) Presynaptic GABAA receptors enhance transmission and LTP induction at hippocampal mossy fiber synapses. Nat Neurosci 13: 431–438.
19. Pugh JR, Jahr CE (2011) Axonal GABAA receptors increase cerebellar granule cell excitability and synaptic activity. J Neurosci 31: 565–574.
20. Hu W, Shu Y (2012) Axonal bleb recording. Neurosci Bull 28: 342–350.
21. Barker JL, McBurney RN, MacDonald JF (1982) Fluctuation analysis of neutral amino acid responses in cultured mouse spinal neurones. J Physiol 322: 365–387.
22. Neher E, Stevens CF (1977) Conductance fluctuations and ionic pores in membranes. Annu Rev Biophys Bioeng 6: 345–381.
23. Lv XH, Zhan C, Zeng SQ, Chen WR, Luo QM (2006) Construction of multiphoton laser scanning microscope based on dual-axis acousto-optic deflector. Rev Sci Instrum 77.
24. Ruiz A, Fabian-Fine R, Scott R, Walker MC, Rusakov DA, et al. (2003) GABAA receptors at hippocampal mossy fibers. Neuron 39: 961–973.
25. Howe JR, Sutor B, Zieglgansberger W (1987) Baclofen reduces post-synaptic potentials of rat cortical neurones by an action other than its hyperpolarizing action. J Physiol 384: 539–569.
26. Freund TF, Buzsaki G (1996) Interneurons of the hippocampus. Hippocampus 6: 347–470.
27. Somogyi P, Tamas G, Lujan R, Buhl EH (1998) Salient features of synaptic organisation in the cerebral cortex. Brain Res Brain Res Rev 26: 113–135.
28. Geiger JR, Jonas P (2000) Dynamic control of presynaptic Ca(2+) inflow by fast-inactivating K(+) channels in hippocampal mossy fiber boutons. Neuron 28: 927–939.
29. Augustine GJ (1990) Regulation of transmitter release at the squid giant synapse by presynaptic delayed rectifier potassium current. J Physiol 431: 343–364.
30. Trigo FF, Marty A, Stell BM (2008) Axonal GABAA receptors. Eur J Neurosci 28: 841–848.
31. Eccles JC, Eccles RM, Magni F (1961) Central inhibitory action attributable to presynaptic depolarization produced by muscle afferent volleys. J Physiol 159: 147–166.
32. Turecek R, Trussell LO (2002) Reciprocal developmental regulation of presynaptic ionotropic receptors. Proc Natl Acad Sci U S A 99: 13884–13889.
33. Pouzat C, Marty A (1999) Somatic recording of GABAergic autoreceptor current in cerebellar stellate and basket cells. J Neurosci 19: 1675–1690.
34. Tachibana M, Kaneko A (1987) gamma-Aminobutyric acid exerts a local inhibitory action on the axon terminal of bipolar cells: evidence for negative feedback from amacrine cells. Proc Natl Acad Sci U S A 84: 3501–3505.

35. Debanne D (2004) Information processing in the axon. Nat Rev Neurosci 5: 304–316.
36. Christie JM, Jahr CE (2009) Selective expression of ligand-gated ion channels in L5 pyramidal cell axons. J Neurosci 29: 11441–11450.
37. Khirug S, Yamada J, Afzalov R, Voipio J, Khiroug L, et al. (2008) GABAergic depolarization of the axon initial segment in cortical principal neurons is caused by the Na-K-2Cl cotransporter NKCC1. J Neurosci 28: 4635–4639.
38. Golding NL, Oertel D (1996) Context-dependent synaptic action of glycinergic and GABAergic inputs in the dorsal cochlear nucleus. J Neurosci 16: 2208–2219.
39. Martina M, Royer S, Pare D (2001) Cell-type-specific GABA responses and chloride homeostasis in the cortex and amygdala. J Neurophysiol 86: 2887–2895.
40. Chavas J, Marty A (2003) Coexistence of excitatory and inhibitory GABA synapses in the cerebellar interneuron network. J Neurosci 23: 2019–2031.
41. Wagner S, Castel M, Gainer H, Yarom Y (1997) GABA in the mammalian suprachiasmatic nucleus and its role in diurnal rhythmicity. Nature 387: 598–603.
42. Payne JA, Rivera C, Voipio J, Kaila K (2003) Cation-chloride co-transporters in neuronal communication, development and trauma. Trends Neurosci 26: 199–206.
43. Ben-Ari Y, Gaiarsa JL, Tyzio R, Khazipov R (2007) GABA: a pioneer transmitter that excites immature neurons and generates primitive oscillations. Physiol Rev 87: 1215–1284.
44. Vardi N, Zhang LL, Payne JA, Sterling P (2000) Evidence that different cation chloride cotransporters in retinal neurons allow opposite responses to GABA. J Neurosci 20: 7657–7663.
45. Kullmann DM, Ruiz A, Rusakov DM, Scott R, Semyanov A, et al. (2005) Presynaptic, extrasynaptic and axonal GABAA receptors in the CNS: where and why? Prog Biophys Mol Biol 87: 33–46.
46. Rudomin P, Schmidt RF (1999) Presynaptic inhibition in the vertebrate spinal cord revisited. Exp Brain Res 129: 1–37.
47. Cattaert D, El Manira A (1999) Shunting versus inactivation: analysis of presynaptic inhibitory mechanisms in primary afferents of the crayfish. J Neurosci 19: 6079–6089.
48. Segev I (1990) Computer study of presynaptic inhibition controlling the spread of action potentials into axonal terminals. J Neurophysiol 63: 987–998.
49. Chiang PH, Wu PY, Kuo TW, Liu YC, Chan CF, et al. (2012) GABA is depolarizing in hippocampal dentate granule cells of the adolescent and adult rats. J Neurosci 32: 62–67.
50. Gulledge AT, Stuart GJ (2003) Excitatory actions of GABA in the cortex. Neuron 37: 299–309.
51. Mody I, De Koninck Y, Otis TS, Soltesz I (1994) Bridging the cleft at GABA synapses in the brain. Trends Neurosci 17: 517–525.
52. Mozrzymas JW (2004) Dynamism of GABA(A) receptor activation shapes the "personality" of inhibitory synapses. Neuropharmacology 47: 945–960.
53. Santhakumar V, Hanchar HJ, Wallner M, Olsen RW, Otis TS (2006) Contributions of the GABAA receptor alpha6 subunit to phasic and tonic inhibition revealed by a naturally occurring polymorphism in the alpha6 gene. J Neurosci 26: 3357–3364.
54. Cavelier P, Hamann M, Rossi D, Mobbs P, Attwell D (2005) Tonic excitation and inhibition of neurons: ambient transmitter sources and computational consequences. Prog Biophys Mol Biol 87: 3–16.
55. Semyanov A, Walker MC, Kullmann DM, Silver RA (2004) Tonically active GABA A receptors: modulating gain and maintaining the tone. Trends Neurosci 27: 262–269.
56. Farrant M, Nusser Z (2005) Variations on an inhibitory theme: phasic and tonic activation of GABA(A) receptors. Nat Rev Neurosci 6: 215–229.
57. Shu Y, Duque A, Yu Y, Haider B, McCormick DA (2007) Properties of action-potential initiation in neocortical pyramidal cells: evidence from whole cell axon recordings. J Neurophysiol 97: 746–760.
58. Yang J, Ye M, Tian C, Yang M, Wang Y, et al. (2013) Dopaminergic modulation of axonal potassium channels and action potential waveform in pyramidal neurons of prefrontal cortex. J Physiol 591: 3233–3251.
59. Alle H, Geiger JR (2008) Analog signalling in mammalian cortical axons. Curr Opin Neurobiol. 2008/09/20 ed. 314–320.
60. Bischofberger J, Geiger JR, Jonas P (2002) Timing and efficacy of Ca2+ channel activation in hippocampal mossy fiber boutons. J Neurosci 22: 10593–10602.